Galvanomagnetic Effects and Band Structure of Pure and Tin-Doped Single-Crystal Antimony*

SEYMOUR EPSTEIN
U. S. Army Electronics Research and Development Laboratory, Ft. Monmouth, New Jersey

AND

H. J. JURETSCHKE†
Polytechnic Institute of Brooklyn, Brooklyn, New York

(Received 10 September 1962)

Room-temperature resistivities, Hall coefficients, and magnetoresistivities at low magnetic fields are presented for unworked, preshaped, oriented single-crystal rods of 0.8 and 0.2% tin-doped and pure antimony grown at a fast rate. The data are interpreted in terms of two threefold sets of tilted mobility ellipsoids for the valence and conduction bands. For pure antimony our analysis yields an anisotropic hole and electron structure, in essential agreement with the result of an earlier analysis of somewhat different values for the same coefficients, and, in addition, an alternative structure for electrons. The alloy data are compatible with these ellipsoids upon isotropic scaling of the mobilities of each band and upon specifying unequal carrier densities. The latter show that each tin atom removes 0.3 carrier and that, if nonshifting overlapping bands of standard and inverted form and degenerate statistics apply, the hole band is 2.2 times as dense as the electron band at the Fermi energy for pure antimony. For 0.8% tin-doped antimony the ratio is 3.9, and about 2% tin should be needed for conduction by holes alone. By ascribing Shoenberg's de Haas-Van Alphen effective masses to the electrons, the band edge overlap is 0.19 eV and the hole Fermi energy is 0.06 eV for pure antimony; by ascribing them to holes, the corresponding values are 0.42 and 0.13 eV, respectively.

I. INTRODUCTION

IN the recent paper of Freedman and Juretschke[1] (hereinafter designated by F-J), the 12 phenomenologically independent coefficients which describe antimony's electrical conduction in the presence of weak magnetic fields were measured and interpreted in terms of a nine-parameter, general multivalley model of the valence and conduction bands. Their analysis leads to an ellipsoidal band structure of electrons overlapping from an otherwise full Brillouin zone into the next higher one by 10^{-3} carriers/atom (3.7×10^{19}/cm^3), the same number as obtained by Shoenberg[2] from de Haas-Van Alphen (dHvA) data. This report extends the same method to the determination of the galvanomagnetic coefficients of tin-doped antimony and their interpretation in terms of F-J's model, generalized to unequal hole and electron populations.

Browne and Lane[3] had shown that 0.1% of tin seemed to suffice to bring the alloy into the region of one-carrier conduction. Therefore, tin was added in amounts of 0.2 and 0.8%. These selections are somewhat arbitrary since it is known that, on alloying, the carrier contribution per added atom is not necessarily the difference in the valency of the solute and antimony or bismuth.[4] In addition to studying these alloys, measurements on pure antimony were repeated to establish a reference for the alloy data based on pure crystals grown by the same method.[5] Both the method of growth and the specimen preparation differ from F-J, and actually lead to some differences in electrical properties.

In Sec. II the low-magnetic-field resistivity tensor components are presented, and expressions are given for the magnetic-field-dependent electric fields which form the basis of our measurements. Some experimental details are highlighted in Sec. III, and, in Sec. IV, the phenomenological coefficients are deduced from the experimental data. In Sec. V the basic model is reviewed, the procedure for fitting its parameters to the experimental numbers is outlined, and the results of this procedure are given. These results are also discussed and interpreted in terms of simple ellipsoidal energy bands of standard form with degenerate carrier populations.

II. DESIGN OF EXPERIMENTS

For antimony, of symmetry $R\bar{3}m$, Ohm's law connecting electric fields E_i and current densities J_j takes the form

$$E_i=\rho_{ij}(H)J_j. \quad (1)$$

If each resistivity tensor component $\rho_{ij}(H)$ can be expanded in terms of a rapidly converging series of increasing powers of the magnetic field, 12 independent coefficients are required to describe the isothermal galvanomagnetic effects up to second order in H[6]. These coefficients are most conveniently presented and defined

* Based on a dissertation of the same title submitted in fulfilment of the thesis requirement for the Ph.D. degree at the Polytechnic Institute of Brooklyn (1961).

† Work supported in part by the U. S. Office of Naval Research.

[1] S. J. Freedman and H. J. Juretschke, Phys. Rev. **124**, 1379 (1961).

[2] D. Shoenberg, Proc. Roy. Soc. (London) **A 245**, 1 (1952).

[3] S. H. Browne and C. T. Lane, Phys. Rev. **60**, 895 (1941); **60**, 899 (1941).

[4] D. Shoenberg and M. Z. Uddin, Proc. Roy. Soc. (London) **156**, 687 (1936); V. Heine, *ibid.* **A69**, 505 (1956); D. Weiner, Phys. Rev. **125**, 1226 (1962).

[5] Seymour Epstein, J. Electrochem. Soc. **109**, 738 (1962).

[6] H. J. Juretschke, Acta. Cryst. **8**, 716 (1955); T. Okada, Mem. Faculty Sci., Kyushu University, **B1**, 157 (1955).

by the following expressions for each $\rho_{ij}(H)$.

$$\begin{aligned}
\rho_{11}(H)&=\rho_{11}+A_{11}H_1^2+A_{12}H_2^2+A_{13}H_3^2-2A_{24}H_2H_3,\\
\rho_{22}(H)&=\rho_{11}+A_{12}H_1^2+A_{11}H_2^2+A_{13}H_3^2+2A_{24}H_2H_3,\\
\rho_{33}(H)&=\rho_{33}+A_{31}H_1^2+A_{31}H_2^2+A_{33}H_3^2,\\
\rho_{23}(H)&=R_{231}H_1-A_{42}H_1^2+A_{42}H_2^2+2A_{44}H_2H_3,\\
\rho_{31}(H)&=R_{231}H_2-2A_{42}H_2H_3+2A_{44}H_1H_3,\\
\rho_{12}(H)&=R_{123}H_3-2A_{24}H_1H_3+(A_{11}-A_{12})H_1H_2.
\end{aligned}\tag{2}$$

The remaining components of $\rho_{ij}(H)$ follow from the Onsager relation, $\rho_{ij}(H)=\rho_{ji}(-H)$.

This description applies with respect to an orthogonal coordinate system having 1 (or X) along the binary axis, 2 (or Y) along the bisectrix axis, and 3 (or Z) along the threefold rotation-inversion axis. The coefficients ρ_{ij}, $-R_{ijk}$, A_{ij} are the resistivities, the Hall constants, and the generalized magnetoresistance (MR) constants; they are determined experimentally by measuring the electric field accompanying a given current flow in the presence of a magnetic field. With long, oriented single-crystal rods of rectangular cross section, where current flow is uniform, convenient electric field components are chosen parallel and transverse to the current direction and in or across the lateral faces. Various directions of the magnetic field are used to separate the contributions of the various coefficients for a given crystal.

Our experimental configurations differ from those described by Juretschke,[6] and used by F-J. Rotations of the magnetic field both in a plane parallel to the current and the Z axis and in a plane normal to the current reduce the minimum number of differently oriented single-crystal rods necessary to determine the 12 coefficients to two. Convenient orientations are that the axis is either normal (the 90° orientation) or parallel (the 0° orientation) to the rod axis, which defines the direction of current flow. The corresponding configurations are called $J\perp c$ and $J\|c$ and are depicted in Fig. 1 where the plane of rotation of H is shown at an arbitrary angle η from the $Y-Z$ mirror plane. In both configurations H is rotated through angles ϕ from the c axis in a plane containing this axis. Equations (1) and (2) specialize to Eqs. (3), (4), (5), and (6), described below for the two configurations.

(a) $J\perp c$ Orientation [Fig. 1(a)]

Here the three mutually perpendicular electric fields measured are E_J, the longitudinal field in the J direction; E_Z, the transverse field in the Z direction; and $E_{Z\times J}$, the transverse field in the $Z\times J$ direction. In terms of the angles of Fig. 1(a) the expressions for these fields up to second powers of H are for $\eta=\theta$

$$\begin{aligned}
E_J&=\rho_{11}J+JH^2(A_{12}\sin^2\phi+A_{13}\cos^2\phi\\
&\qquad -A_{24}\cos3\theta\sin2\phi);\\
E_Z&=JHR_{231}\sin\phi+JH^2A_{42}\sin3\theta\sin^2\phi;\\
E_{Z\times J}&=-JHR_{123}\cos\phi+JH^2A_{24}\sin3\theta\sin2\phi.
\end{aligned}\tag{3}$$

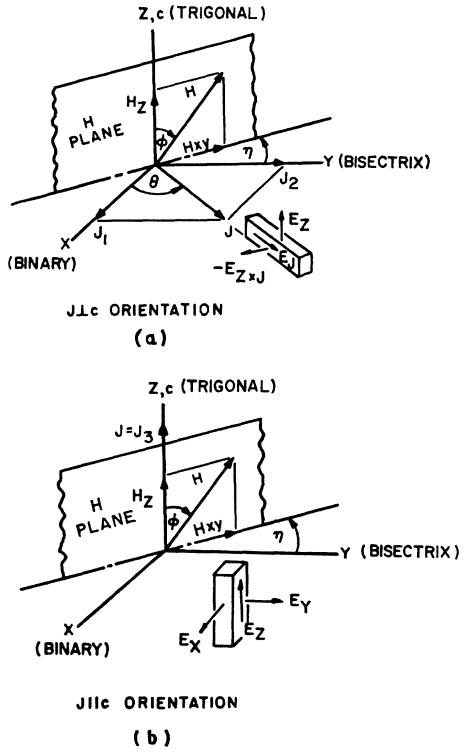

FIG. 1. Experimental configurations giving specimen orientations and directions of current, applied magnetic field, and measured galvanomagnetic fields relative to crystallographic axes.

The binary axis is chosen at an angle θ, not equal to zero, since some of the terms including third-order ones can contribute only under these conditions. The dependence of these fields on ϕ permits the separation of the measured field into contributions from the various individual terms. A_{24} appears in two fields, and will give comparable contributions in both for $\theta=\pm15°$. Seven coefficients, ρ_{11}, R_{231}, R_{123}, A_{12}, A_{13}, A_{24}, and A_{42}, result. For $\eta=\theta+\pi/2$, the fields are

$$\begin{aligned}
E_J&=\rho_{11}J+JH^2(A_{11}\sin^2\phi+A_{13}\cos^2\phi\\
&\qquad +A_{24}\sin3\theta\sin2\phi);\\
E_Z&=JH^2(-A_{42}\sin3\theta\sin^2\phi-A_{44}\sin2\phi);\\
E_{Z\times J}&=-JHR_{123}\cos\phi+JH^2A_{24}\cos3\theta\sin2\phi.
\end{aligned}\tag{4}$$

This arrangement yields the additional coefficients A_{44} and A_{11}; the remaining coefficients may again be determined, and the agreement of these values with the previously obtained ones serves as a check.

(b) $J\|c$ Orientation [Fig. 1(b)]

For this case H is again rotated in a plane containing J. The three mutually perpendicular fields are:

$$E_J=\rho_{33}J+JH^2(A_{31}\sin^2\phi+A_{33}\cos^2\phi);$$
$$E_X=-JHR_{231}\cos\eta\sin\phi+JH^2(A_{42}\sin2\eta\sin^2\phi-A_{44}\sin\eta\sin2\phi); \quad (5)$$
$$E_Y=JHR_{231}\sin\eta\sin\phi+JH^2(A_{42}\cos2\eta\sin^2\phi+A_{44}\cos\eta\sin2\phi).$$

The three as yet undetermined coefficients, ρ_{33}, A_{31}, and A_{33}, are obtained from E_J, which is independent of η. Here, the lateral rod faces are chosen to be X and Y planes and η is set at either 0° or 90°.

E_X and E_Y permit additional, independent determinations of R_{231}, A_{42}, and A_{44}. These coefficients are also obtainable from the $J\perp c$ oriented rods. The agreement of these two determinations measures the compatibility of the differently oriented samples and, hence, of the entire set of coefficients for each alloy. An additional arrangement in which H is rotated in a plane normal to J can be used as another check. The coefficients R_{231}, A_{42}, and A_{31} enter under these conditions.

Since expressions (3) to (5) are not invariant under the operation $\theta\rightarrow\theta+\pi$ because the signs of A_{24} and A_{42} change, the X and Y axes are not uniquely defined. A consistent but arbitrary choice of axes is made by relating their directions to the intersections of dominant secondary cleavage planes with the c faces and to the slope of the secondary cleavage planes. For these axes, A_{24} and A_{42} are both negative.

III. EXPERIMENTAL DETAIL

Since antimony cleaves easily, preparing specimens by cutting large ingots was given up in favor of recrystallizing molten precast rods of the desired shape in the two principal orientations, a technique long used for bismuth.[7] The slow growth rate prescribed by Kapitza and Hasler, and used by Rausch for circular cylindrical antimony rods,[8] was found to be not conducive to growth in the crystallographic c-axis direction, and led us to a modified apparatus and procedure whereby relatively unstrained and uniformly doped, square (3 mm×3 mm), long (6 cm or more), single-crystal antimony rods with axes along or normal to the c axis can be easily and consistently grown.[5] The technique introduces a very fast rate of crystallization, somewhere between 2 and 10 cm/min, in a crucible material of low heat conductivity relative to antimony. The undoped antimony is 99.997% pure and is used as supplied by the Bradley Mining Company, San Francisco, California from their Yellow Pine Mine at Stibnite, Idaho. Chemically pure Baker's tin is the dopant. We determine the amount of tin added by weighing each mixture before and after alloying, and by spectroscopic sampling.

The crystals selected for measurement show a resistivity between room and liquid nitrogen temperatures comparable with the best data reported in the literature,[9,10] and their galvanomagnetic (GM) coefficients reproduce from crystal to crystal for a given orientation and for the two orientations for $-R_{231}$, $-A_{42}$, $-A_{44}$.

Specimens 20 mm long are sharply cleaved from the longer rods. A set of three probes is placed in the unworked center region far from the ends[11] on each pair of opposite faces. Each probe is accurately aligned on the center line of its face and the two longitudinally displaced probes on a face are separated by about 5 mm. The uncertainty in the geometric factors entering the determination of the electric fields is about 3% for longitudinal and 1.5% for transverse effects. All voltage probes, No. 35 or No. 40 copper wire, are spot welded. Care is taken in all electrical connections to avoid contact emf's. In addition, the contacts and the rods are immersed in an isothermal alcohol bath.

Magnetic fields are obtained from a Varian V-4007 system. A slightly underdamped high-sensitivity reflecting-type galvanometer (Leeds & Northrop Type HS, Model 2284b) is used for GM measurements, in conjunction with a Wenner thermocouple potentiometer (L & N Cat. No. 7559) to provide stable compensating voltages for the longitudinal effects, and to provide galvanometer calibration voltages. The system sensitivity is between 17 and 25 mm deflection/μV. Primary currents are determined from the voltage drop across a standard 0.01-Ω resistor to one part in 10^4, the drift being reset by hand; the current density is 12 A/cm^2. We define the galvanometer zero as the deflection position which does not change upon reversing the primary current direction in zero magnetic field. Deflections from this point with the magnetic field (and primary current) applied are measures of the transverse fields.

Readings for the longitudinal resistance are obtained for forward and reverse current and are averaged. The unaveraged readings are usually subject to a correction of no more than 1 μV in 300, because of a residual longitudinal temperature gradient due to the current. Longitudinal magnetoresistance values are obtained as follows. For a given current direction the resistance part of the longitudinal voltage is cancelled by applying a potentiometer voltage. The galvanometer reading is noted before, after, and while the magnet is on, the current being kept constant to one part in 10^4 for each reading, and the average deflection is used. In all, four such averages are obtained, $\pm H$ at a given ϕ and $\phi+\pi$, and these are appropriately combined.

Tranverse Hall and magnetoresistance readings are obtained for a given combination of $\pm H$, ϕ, and $\phi+\pi$ for $\pm J$ and averaged to minimize the effect of drift in the bridge balance point. The forward and reverse current averages for $+H$ and ϕ and $-H$ and $\phi+\pi$ are again averaged.

[7] P. Kapitza, Proc. Roy. Soc. (London) **A119**, 358 (1928); L. Schubnikow, Koninkl. Ned. Akad. Amsterdam Proc. **33**, 327 (1930); M. F. Hasler, Rev. Sci. Instr. **4**, 656 (1933).
[8] K. Rausch, Ann. Physik **1**, 190 (1947).
[9] P. W. Bridgman, Proc. Am. Acad. Arts Sci. **60**, 305 (1924).
[10] C. T. Lane and W. A. Dodd, Phys. Rev. **61**, 183 (1942).
[11] J. Volger, Phys. Rev. **79**, 1023 (1950).

IV. EXPERIMENTAL ANALYSIS AND RESULTS

Representative data for various runs and specimens in the arrangements of Sec. II are shown in Figs. 2, 5, and 6. These curves usually include averaging over current direction and correction for misalignment. Figure 2 shows the variation of the transverse fields E_Z and $E_{Z\times J}$ with ϕ for 3.0, 3.5, 4.0, 4.5, 5.0 kG. The magnetic field is rotated in a plane normal to J, and J is normal to c. The theoretically expected variation, the last two of Eqs. (3), is also indicated. The differences for $+H$ and $-H$ curves are related to even effects. How the four constants $-R_{123}$, $-R_{231}$, A_{24}, A_{42} are obtained from these data is exemplified in Figs. 3 and 4. Plotting the differences $[E_Z(H)-E_Z(-H)]/2J$ and $[E_{Z\times J}(H)-E_{Z\times J}(-H)]/2J$ against, respectively, $H\sin\phi$ and $H\cos\phi$, we obtain the straight lines of Fig. 3 whose slopes give the constants $-R_{231}$ and $-R_{123}$. In a similar manner, the sum fields are used to obtain $-A_{24}$ and $-A_{42}$ as shown in Fig. 4.

The data for all H of Fig. 2 fall on straight lines, indicating that the relevant expressions of Eqs. (3) are exact representations and that higher order galvanomagnetic effects are absent in this whole range of magnetic fields. All straight lines pass through the origin, a confirmation of successful systematic removal of misalignment effects.

Figure 5 shows the transverse field E_Z at 5000 G for the case $J\perp c$, $H\perp(Z\times J)$, described by Eqs. (3). The two contributions to this field may be separated as indicated in the figure; the solid curves give the best fit of the theoretically expected variation to the measured points. It should be noted that here the ordinate scale is particularly small.

The angular variation of the longitudinal field E_J for $H\perp J\perp c$, described by Eqs. (2), is shown in Fig. 6(a), curve (A). In this instance, values for A_{12}, A_{13}, and A_{24} are determined from the amplitudes at $\phi=0°$, 45°, 90°, 135° of a smooth curve drawn through the experimental points. To verify that the over-all shape of the curve agrees with theoretical expectation, E_J is computed

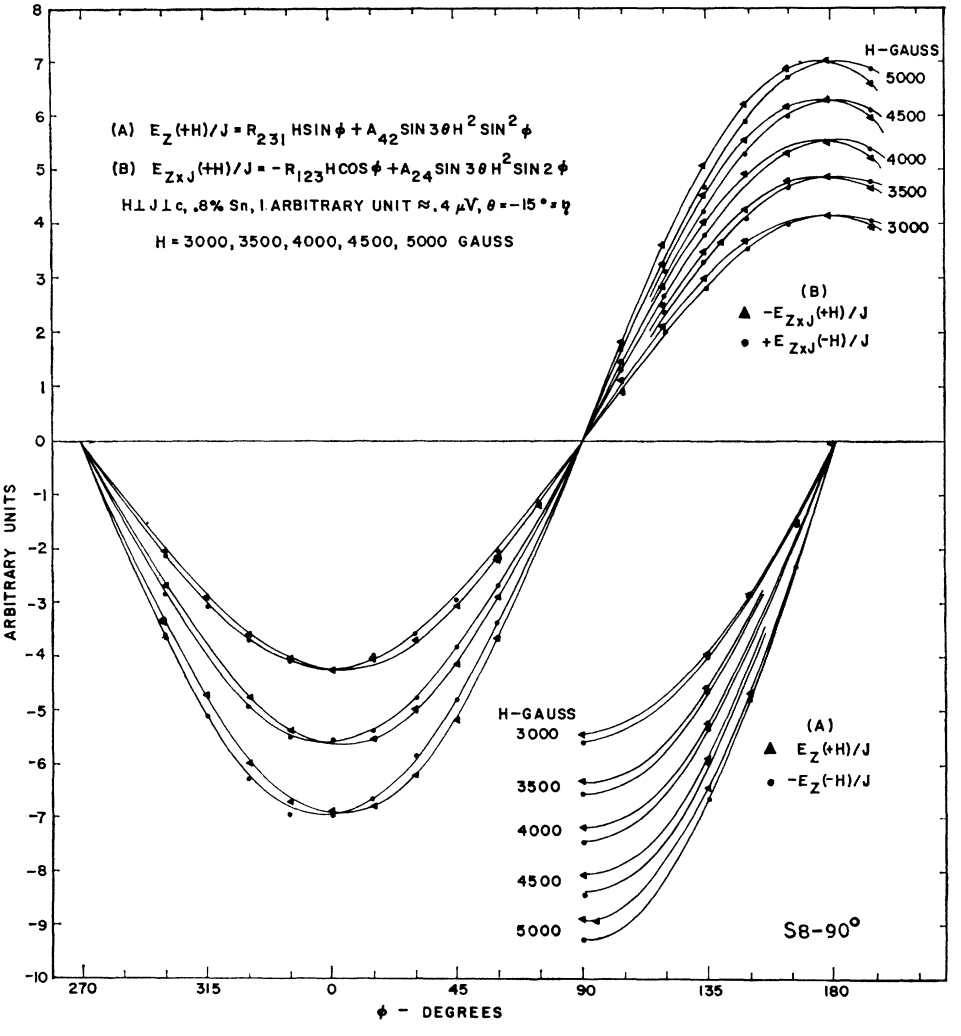

FIG. 2. Transverse galvanomagnetic fields, E_Z and $E_{Z\times J}$, for normal and reverse magnetic fields, $\pm H$, at various angles ϕ and magnetic field strengths. Here, $H\perp J\perp c$.

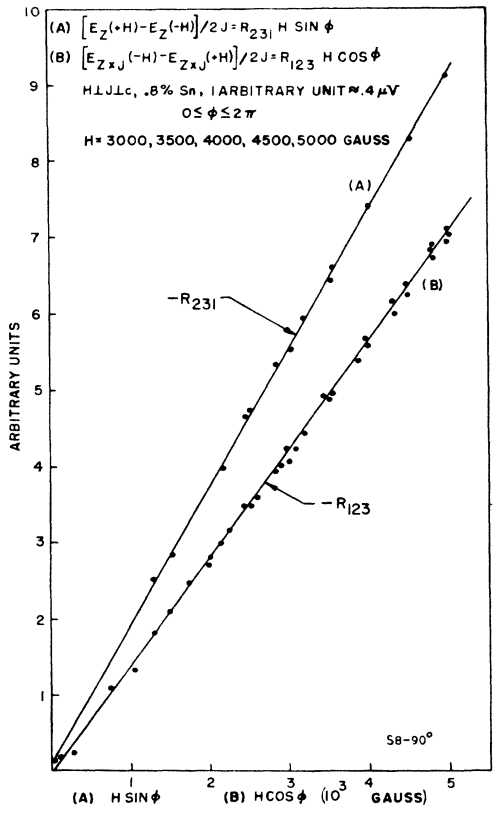

FIG. 3. Analysis of the data of Fig. 2 into difference fields at the various angles ϕ to obtain the Hall constants $-R_{231}$ and $-R_{123}$.

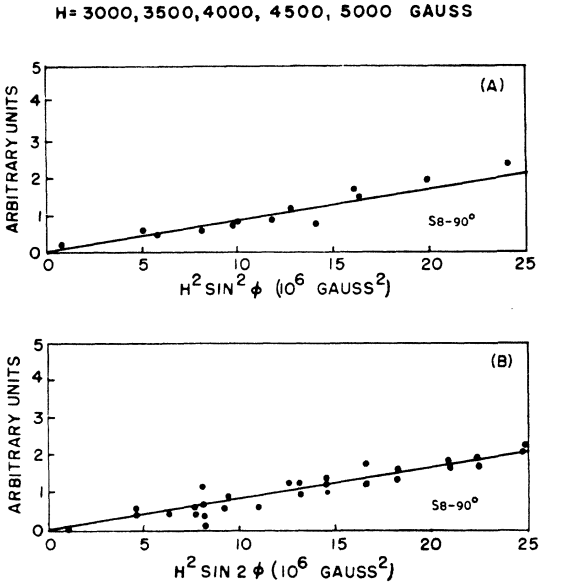

FIG. 4. Analysis of the data of Fig. 2 into sum fields to obtain the magnetoresistance constants $-A_{24}$ and $-A_{42}$.

with these values at other angles where data are taken and compared with the corresponding experimental value. Curve (B) plots E_J calculated vs E_J experimental for these points, the line with slope of unity going through the origin indicating satisfactory agreement. The expected linear dependence of the voltage on H^2 is verified in Fig. 6(b) at the angles of ϕ which allow A_{12} and A_{13} to contribute separately. The values and magnetic-field dependence of A_{11}, A_{33}, and A_{31} are obtained in an analogous manner using the appropriate E_J of Eqs. (4) and (5). With these configurations A_{13} and A_{24} are usually again evaluated as a check, and R_{231}, A_{42}, A_{44} are obtained in order to establish compatibility of the differently oriented specimens. For these three, E_X and E_Y of Eqs. (5) apply.

Typical complete sets of data for one concentration are shown in Table I. The specified limits of reproducibility result mostly from the variation in specimen coefficient value with different experimental determinations. That for $-A_{44}$ is estimated not to exceed 0.06 parts. The minimum accuracy for comparing values of like coefficients for the different specimens, already indicated in Sec. III, is ±1.5% for $-R_{123}$, $-R_{231}$, A_{42}, A_{44}, and ±3% for the remaining ones.

TABLE I. Specimen galvanomagnetic coefficients for undoped antimony.

Phen. coef.[a]	Specimen identification number S1−90°	S2−90°	S3−90°	S1−0°	S2−0°	S3−0°
ρ_{11}	45.2 ±0.8	44.7 ±0.2	44.0 ±0.3	...	...	...
ρ_{33}	...	...	...	33.4 ±1.2	34.9 ±1	35.1 ±0.2
$-R_{231}$	2.04±0.00	2.07±0.05	1.99±0.00	2.05±0.05	2.06±0.00	2.04±0.00
$-R_{123}$	2.32±0.02	2.34±0.00	2.36±0.03	...	...	...
A_{12}	16.00±0.00	16.82±0.00	16.06±0.02	...	...	...
A_{13}	4.66±0.02	5.03±0.03	5.3 ±0.2	...	...	...
A_{31}	...	...	...	10.6 ±0.3	10.8 ±0.2	11.1 ±0.1
A_{11}	6.5 ±0.1	6.79±0.03	6.6 ±0.1	...	...	...
A_{33}	...	...	...	1.95±0.12	2.01±0.04	2.08±0.00
$-A_{44}$	1.48	1.73	1.34	1.56	1.40	1.41
$-A_{24}$	2.75±0.06	2.3 ±0.4	2.73±0.05	...	...	...
$-A_{42}$	2.0 ±0.2	2.06±0.06	2.1 ±0.5	2.24	2.23±0.06	2.25

[a] Units: ρ, 10^{-6} Ω-cm; R, 10^{-10} Ω-cm/G; A, 10^{-15} Ω-cm/G^2.

It is evident from Table I that the limit of reproducibility for a particular coefficient varies from specimen to specimen and is different for the different coefficients on a given specimen. Although this may be due to fluctuations in the composition of the crystal specimens, differences in probe contact properties are their most probable cause. Systematic variations from specimen to specimen in some of the alloy coefficients suggest slight differences in specimen doping concentration.

An additional source of error is the small longitudinal thermal gradients observed on some current-carrying specimens. Such effects and the resulting thermomagnetic effects of the same symmetry as the isothermal galvanomagnetic effects are most likely small since truly systematic variations from specimen to specimen are not observed.

Because the coefficient values for specimens of a given tin concentration seem to fluctuate and because the data of any one specimen are equally likely to be correct, representative values are averages of all data taken. Our choice for representative values and their limits, are presented in Table II which also includes the pure

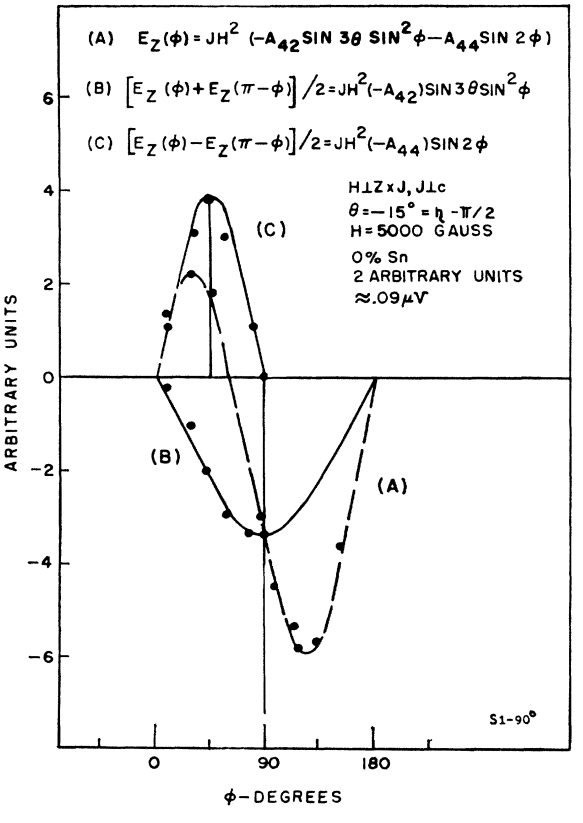

FIG. 5. Transverse galvanomagnetic field E_Z for various ϕ and $H=5000$ G, curve and Eq. (A), and analysis of E_Z into sums and differences, curves and Eqs. (B) and (C), respectively, to obtain $-A_{44}$ and $-A_{42}$. In this case, H is always normal to the $Z\times J$ direction.

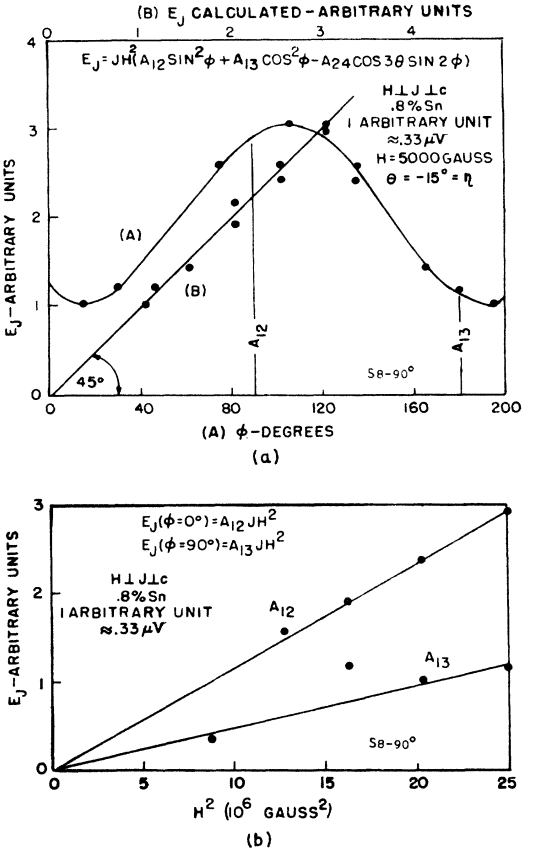

FIG. 6. (a) Curve (A): Longitudinal galvanomagnetic field E_J for various ϕ (lower abscissa) and $H=5000$ G, showing amplitudes and angles used to evaluate A_{12} and A_{13}. The lack of symmetry about these points results from A_{24}'s contribution. Curve (B): E_J observed vs E_J calculated (upper abscissa) at remaining angles to verify formula shown. (b) Demonstration of H^2 dependence of magnetoresistive fields associated with A_{12} and A_{13}, typical for A_{11}, A_{33}, A_{31}, and $-A_{44}$.

antimony values of F-J. These data are next compared with known published values.

For pure antimony, our results reproduce the measurements of ρ_{11} and ρ_{33} by Bridgman[9] and by F-J, but our Hall and most of magnetoresistance constants are lower than F-J's by 10 and by about 20%, respectively. Our lower values may be due to real differences in properties of our regrown precast and their cut crystals, or due to differing measurement techniques. That the difference in results are not merely due to systematic error in current or field measurement is seen by the large fluctuation among the individual magnetoresistance coefficients about this average reduction. For $-A_{44}$ an unusually large discrepancy obtains which we ascribe mainly to the fact that in the work of F-J $-A_{44}$ is calculated from separate measurements on three differently oriented crystals. In this work $-A_{44}$ is more directly evaluated; moreover, it is twice obtained from separate measurements on differently oriented specimens, and the resulting values agree.

TABLE II. Representative pure and doped antimony coefficients.[a]

% tin	Resistivity ρ_{11}	ρ_{33}	Hall $-R_{231}$	$-R_{123}$	Magnetoresistivity A_{12}	A_{13}	A_{31}	A_{11}	A_{33}	$-A_{44}$	$-A_{24}$	$-A_{42}$
0, F-J[b]	43	36, 44	2.2	2.51	19.9	6.4	13.6	7.3	5.2	2.8	3.5	1.4
0	44.3	34.6	2.05	2.34	16.5	5.1	10.8	6.6	2.0	1.5	2.6	2.1
0.2	41.8	38.4	2.07	2.10	11.8	3.6	9.3	4.9	1.8	1.1	2.1	1.7
0.8	38.7	44.4	1.74	1.34	4.4	1.8	5.1	1.95	1.07	0.44	1.0	0.85
Tot. ±%	4	6	5	5	8	8	4	5	10	20	25	25

[a] Units: ρ, 10^{-6} Ω-cm; R, 10^{-10} Ω-cm/G; A, 10^{-15} Ω-cm/G^2.
[b] See reference 1.

Without a systematic comparison of both sets of crystals it is difficult to ascribe the discrepancies to a single cause, and neither set of values for pure antimony has been fully established as the better one. However, since it is felt that we have introduced a more systematic approach towards growing and handling the crystals, and towards reproducibly preparing and measuring specimens, our pure antimony data are to be preferred.

With respect to the alloys, the only data in the literature refer to the variation of ρ_{11} with tin doping. In agreement with Lane and Dodd,[10] at room temperature ρ_{11} decreases and at liquid-nitrogen temperature it increases with increasing tin content for concentrations in our range. We also duplicate their variation in ρ_{11} with temperature for pure and 0.2% doped antimony over this temperature range. Our 0.8% alloy, however, corresponds to their 0.5% alloy. Unfortunately, no other data exist giving the variation of the remaining coefficients on alloying. However, the regular decrease in the magnetoresistivities and Hall coefficients, the former faster than the latter, is in agreement with what one would expect if the number of majority carriers increases while the scattering time and mobilities decrease faster with changes in Fermi level. The fact that ρ_{33} increases while ρ_{11} decreases, and that one of the Hall coefficients increases slightly before decreasing, suggests that a more detailed explanation must also include minority carriers. The model for such an explanation is developed in the following Section.

The inverse galvanomagnetic coefficients needed for theoretical interpretation, and the limits within which fits of the model to the data are explored, are listed in Table III.

V. ELLIPSOIDAL BAND STRUCTURE AND ANALYSIS

This section discusses the interpretation of the experimental data in terms of the ellipsoidal band structure model developed by F-J and also by Drabble and Wolfe[12] and Okada.[12] For application to the alloys, the model has been generalized to include unequal electron and hole carrier populations.

[12] J. R. Drabble and R. Wolfe, Proc. Phys. Soc. (London) **B49**, 1101 (1956); T. Okada, Mem. Faculty Sci., Kyushu University **B1**, 168 (1955).

a. The Basic Model

Surfaces of constant energy in the neighborhood of the Fermi level are represented by a family of three ellipsoids in momentum space. Each ellipsoid is characterized by three principal axes, and an angle of tilt of one principal axis with respect to the $\bar{3}$ axis; symmetry requires one of the axes to lie along a binary direction and the remaining two in the mirror plane. This is, therefore, not the most general ellipsoidal structure. It is the simplest one which does not require any of the phenomenological coefficients measured to vanish identically.

This energy structure is related simply to transport properties by the assumptions that interellipsoid scattering can be neglected, and that within each ellipsoid scattering is describable by a relaxation time tensor $\tau(\mathbf{k})$ diagonal in the principal energy coordinate system. In such a model the observed electrical properties arise from the independent additive contributions of each ellipsoid separately, and the usual definition for the principal mobilities, μ_i, in terms of the principal effective masses, m_i, and principal scattering times, τ_i, applies:

$$\mu_i = e\tau_i/m_i, \tag{6}$$

where $i=1, 2, 3$. For one type of carrier of density N in a family of three ellipsoids the observable inverse galvanomagnetic coefficients are given by the following functions of the mobilities:

$$\begin{aligned}
2\sigma_{11} &= Ne[\mu_1+\alpha^2\mu_2+\beta^2\mu_3],\\
\sigma_{33} &= Ne[\beta^2\mu_2+\alpha^2\mu_3],\\
-2cP_{231} &= \pm Ne[\mu_2\mu_3+\mu_1(\beta^2\mu_2+\alpha^2\mu_3)],\\
-cP_{123} &= \pm Ne[\mu_1(\alpha^2\mu_2+\beta^2\mu_3)],\\
2c^2B_{13} &= Ne[\mu_1+\alpha^2\mu_2+\beta^2\mu_3][\mu_1(\alpha^2\mu_2+\beta^2\mu_3)],\\
2c^2B_{31} &= Ne[\beta^2\mu_2+\alpha^2\mu_3][\mu_2\mu_3+\mu_1(\beta^2\mu_2+\alpha^2\mu_3)],\\
c^2B_4 \equiv c^2(3B_{12}-B_{11}-2B_{44}) &= Ne[\mu_1+\alpha^2\mu_2+\beta^2\mu_3][\mu_2\mu_3+\mu_1(\beta^2\mu_2+\alpha^2\mu_3)],\\
-2c^2B_{44} &= Ne[\beta^2\mu_2+\alpha^2\mu_3][\mu_1(\alpha^2\mu_2+\beta^2\mu_3)],\\
2c^2B_{33} \equiv c^2(-B_{12}+3B_{11}-2B_{44}) &= Ne\alpha^2\beta^2\mu_1(\mu_2-\mu_3)^2,\\
4c^2B_{24} &= Ne\alpha\beta\mu_1(\mu_2-\mu_3)[-\mu_1+\alpha^2\mu_2+\beta^2\mu_3],\\
4c^2B_{42} &= Ne\alpha\beta(\mu_2-\mu_3)[\mu_2\mu_3-\mu_1(\beta^2\mu_2+\alpha^2\mu_3)].
\end{aligned} \tag{7}$$

TABLE III. Representative pure and tin-doped antimony coefficients.

% tin	Conductivity σ_{11} (10^3/Ω-cm)	σ_{33}	Inverse Hall $-P_{231}$ (10^{-1}/Ω-cm-G)	$-P_{123}$	B_{12}	B_{13}	B_{31}	Magnetoconductivity B_{11} (10^{-6}/Ω-cm-G²)	B_{33}	$-B_{44}$	$\pm B_{24}$	$\pm B_{42}$
0, F-J[a]	23.2	27.5	1.44	1.36	11.5	4.2	11.2	4.0	3.9	2.2	1.9	0.87
0	22.6	29.0	1.34	1.19	9.0	3.2	9.9	3.3	1.7	1.4	1.33	1.39
0.2	23.9	26.1	1.25	1.20	7.4	2.6	7.0	2.2	1.2	1.01	1.20	1.06
0.8	25.9	22.5	1.01	0.9	3.4	1.5	3.0	1.3	0.54	0.43	0.66	0.50
Tot. ±%	6	6	17	17	19	24	18	17	22	38	37	37

[a] See reference 1.

For each ellipsoid, the "1" direction is along a binary axis, while "2" and "3" lie in a mirror plane, "3" making an angle ψ with the $\bar{3}$ axis. In the above equations, $\alpha=\cos\psi$, $\beta=\sin\psi$; σ_{ii} are the conductivities; $-P_{ijk}$ are the inverse Hall coefficients; and B_{pq} are the magnetoconductivities.

For more than one carrier the right-hand sides of Eqs. (7) consist of a number of similar contributions. Thus, for two ellipsoid sets characterized by N_1, μ_1, μ_2, μ_3, α_1, β_1 and N_2, ν_1, ν_2, ν_3, α_2, β_2,

$$\begin{aligned} 2\sigma_{11}&=N_1e[\mu_1+\alpha_1^2\mu_2+\beta_1^2\mu_3] \\ &\quad+N_2e[\nu_1+\alpha_2^2\nu_2+\beta_2^2\nu_3], \\ -2cP_{231}&=-N_1e[\mu_2\mu_3+\mu_1(\beta_1^2\mu_2+\alpha_1^2\mu_3)] \\ &\quad+N_2e[\nu_2\nu_3+\nu_1(\beta_2^2\nu_2+\alpha_2^2\nu_3)], \text{ etc.} \end{aligned} \tag{8}$$

The inverse Hall coefficient is written on the assumption that N_2 refers to holes and N_1 to electrons. By the explicit introduction of such signs, all mobilities and densities are always taken as positive.

Equations (7) define all twelve phenomenological constants. If the model contains fewer independent parameters, it requires certain identities among the observed coefficients. The number of such relations depends on the general band structure features. Thus, for two bands, with $N_1=N_2$, the nine independent parameters predict three identities. Two of the identities are known:

$$2B_{33}=3B_{11}-B_{12}-2B_{44} \tag{9}$$

and

$$\begin{aligned} &4P_{231}[\sigma_{11}(-2B_{44})-\sigma_{33}B_{13}] \\ &\quad=P_{123}[4\sigma_{11}B_{31}-\sigma_{33}(3B_{12}-B_{11}-2B_{44})]. \end{aligned} \tag{10}$$

For unequal carrier densities, Eq. (10) no longer holds, and only Eq. (9) and an unknown identity exist. It is of interest, however, that in this case, the difference in carrier densities is easily expressed in terms of observed coefficients. We have

$$(N_2-N_1)ec=\frac{4P_{231}[\sigma_{11}(-2B_{44})-\sigma_{33}B_{13}]-P_{123}[4\sigma_{11}B_{31}-\sigma_{33}(3B_{12}-B_{11}-2B_{44})]}{4B_{13}B_{31}-(-2B_{44})(3B_{12}-B_{11}-2B_{44})}. \tag{11}$$

This is a useful relation for checking the trend of the coefficients with known alloying. If $N_1=0$ we obtain the single carrier case which involves seven identities. All of these are known. Among the useful ones, in addition to Eq. (9), are the two following relations:

$$\begin{aligned} N_2ec&=\sigma_{11}(-P_{123})/B_{13}=\sigma_{33}(-P_{231})/B_{31} \\ &=\sigma_{33}(-P_{123})/(-2B_{44}) \\ &=4\sigma_{11}(-P_{231})/(3B_{12}-B_{11}-2B_{44}), \end{aligned} \tag{12}$$

and

$$4B_{13}B_{31}=(-2B_{44})(3B_{12}-B_{11}-2B_{44}). \tag{13}$$

These identities serve as the first check on the general applicability of the model to the experimental numbers, and may also be used to differentiate between the single or multiple carrier possibilities. The fact, as F-J have noted, that Eqs. (7) require a negative definite value for B_{44} is also of importance.

A possible way of relating the alloy data to pure antimony introduces isotropic scaling of all mobilities of a given carrier, in addition to changes in carrier density. Let r_e represent the ratio of the electron carrier density in the alloy to that in pure antimony and w_e the ratio of each electron mobility in the alloy to the corresponding pure antimony mobility, and define r_h and w_h similarly for holes. The alloy coefficients, in this section denoted by $\sigma_{ii,a}$, $P_{ijk,a}$, $B_{pq,a}$, may be written as

$$\begin{aligned} \sigma_{ii,a}&=r_hw_h\sigma_{ii,h}+r_ew_e\sigma_{ii,e}\equiv a_1\sigma_{ii,h}+b_1\sigma_{ii,e}, \\ -P_{ijk,a}&=-r_hw_h^2P_{ijk,h}+r_ew_e^2P_{ijk,e} \\ &\equiv-a_2P_{ijk,h}+b_2P_{ijk,e}, \\ B_{pq,a}&=r_hw_h^3B_{pq,h}+r_ew_e^3B_{pq,e} \\ &\equiv a_3B_{pq,h}+b_3B_{pq,e}. \end{aligned} \tag{14}$$

Here the pure antimony coefficients with subscripts e or h are, respectively, the electron and hole contributions given by Eqs. (7); a_i and b_i correspond to $r_hw_h^i$ and $r_ew_e^i$ and satisfy

$$a_2^2=a_1a_3, \quad \text{and} \quad b_2^2=b_1b_3. \tag{15}$$

TABLE IV. Mobility and tilt angle ellipsoidal parameters for pure antimony.

Solu. No.	Carrier density N_0 (10^{19}/cm^3)	Holes Mobilities ν_1	ν_2 (10^3 cm^2/V-sec)	ν_3	Tilt angle ψ_ν	Electrons Mobilities μ_1	μ_2 (10^3 cm^2/V-sec)	μ_3	Tilt angle ψ_μ
318	4.3	4.07	0.20	2.4	20°	1.45	0.18	2.68	10°
430	4.3	3.80	0.13	2.42	22°	0.17	1.63	2.43	54°
F-J[a]	3.7	3.56	0.13	3.30	27°	0.15	1.18	4.05	60°

[a] See reference 1.

b. General Ellipsoidal Features of the Results

We consider the application of the various models by determining how well the inverse data, presented in Table III, satisfy the identities and by examining the prediction of the various relations. Trends in the coefficients with increasing alloying are discussed and examined for scaling properties and reasonableness.

The initial and simplest indication of the applicability of the general ellipsoidal model is the negative experimental value of B_{44} for pure and alloyed antimony. We also find, because of the inherently large calculated limits of the inverse data, that the relevant pure and alloy coefficients—B_{24} and B_{42} not included—more or less satisfy the identity relations of each arbitrary specific model within our wide calculated tolerances. Equation (11), nevertheless, does point to a net increase in the effective number of positive carriers, N_2-N_1. For pure and 0.2 and 0.8% tin-doped antimony, there obtains 3.7, 4.6, 8.3×10^{19}/cm^3, respectively, with a tolerance of roughly $\pm200\%$.

The possibility of scaling the alloy coefficients is evident from Table III. On the addition of 0.8% tin σ_{11} increases about 15% and σ_{33} decreases about 22%, while the inverse Hall coefficients and the eight magnetoconductivities, respectively, decrease about 25 and 70% of their corresponding pure antimony values. Similar changes occur for the 0.2% alloy.

These changes are consistent with the scaling model where the B's are most sensitive to alloying and the σ's least. Moreover, the changes are compatible with an increasing hole population ($r_h>1$), a decreasing electron population ($r_e<1$), decreasing hole mobilities ($w_h<1$), and increasing electron mobilities ($w_e>1$) all of which can be reasonably expected to happen on adding tin.

TABLE V. Calculated coefficients for undoped antimony.

Phen. coef.[b]	Solution 318 Calculated	Calc/exp	Solution 430 Calculated	Calc/exp	Solution of F-J[a] Calculated	Calc/exp[c]
σ_{11}	21.2	0.94	22.6	1.00	23.2	1.00
σ_{33}	30.7	1.06	26.9	0.93	27.5	1.00
$-P_{123}$	0.98	0.82	0.98	0.83	1.36	1.00
$-P_{231}$	1.34	1.00	1.34	1.00	1.44	1.00
$2B_{13}$	5.95	0.93	5.84	0.91	8.27	0.97
$2B_{31}$	18.1	0.91	17.0	0.88	21.6	0.96
$-2B_{44}$	2.9	1.04	3.02	1.08	5.01	1.14
B_4	30.1	1.14	30.8	1.16	36.2	1.04
B_{33}	1.33	0.78	1.75	1.00	3.59	0.92
$-4B_{24}$	7.0	1.3	6.86	1.31	7.16	0.94
$-B_{42}$	4.1	0.74	3.29	0.59	3.45	0.99

[a] Reference 1.
[b] Units: σ, 10^3/Ω-cm; P, 10^{-18}/Ω-cm-G; B, 10^{-6}/Ω-cm-G^2.
[c] In this computation of calc/exp, F-J's experimental values are used.

c. Computational Analysis

Although according to the preceding discussion the experimental test of the identities of each of the various models does not rule out any one absolutely, the data are well compatible with two carriers and appear to scale. Hence, we have applied the two equal carrier model to the pure antimony coefficients and then tried to scale the pure antimony electron and hole contributions for the best set of a_i and b_i for each set of alloy data. Obviously, by adopting scaling we neglect possible changes in the energy band structure with doping.

Pure antimony band structure parameters are obtained from the measured coefficients by an IBM 650 computer analysis by means of the program developed by F-J. A modification was introduced to restrict acceptable solutions to those whose computed coefficients are within the calculated tolerance in addition to those having a low weighted mean-square deviation or figure of merit. The two best among the many good solutions found in the same neighborhood are shown in Table IV. They are characterized by highly anisotropic mobilities and nonzero tilt angles, have $N=4.3\times10^{19}$/cm^3, and are remarkably similar in their hole structures. They differ primarily in the size of μ_1 and in the remaining electron ellipsoid parameters. The fits to the data of either solution, shown in Table V, are uneven and neither electron structure can be favored. Consequently, the scaling property of the alloy coefficients in relation to both complete solutions is examined. It is important to note that the common hole solution and electron solution No. 430 are in the same neighborhood already found by F-J with slightly different experimental coefficients.

Alloy solutions are based on scaling of the electrons and hole contributions to the twelve coefficients according to the scheme already outlined. These separate contributions are shown in Table VI. Because their fit to the pure antimony data is not uniform, a scaled alloy fit must be considered satisfactory if it lies within or near compounded limits determined by the experimental

data and the pure antimony agreement. With this adjustment of effective limits of error the scaling consists of finding the best sets of a_i, b_i from an overdetermined set of equations, subject to Eq. (15). Although the solutions are not unique, they fall into well-defined neighborhoods.

Scaled values of the coefficients and the experimental values are shown for the two solutions in Table VII. The quality of the fits is about the same as for pure antimony and the fit is better for the 0.2% alloy than for the 0.8% alloy data. Both pure antimony solutions yield nearly the same scaling factors, though particularly the b_i are not very significant as the electrons contribute relatively little to most coefficients. None the less, all possible combinations of the a_i, b_i yield essentially the same relative changes for the carrier densities and mobilities. The most probable values are summarized in Table VIII. They point to a net increase in positive carriers for the 0.8% tin-doped alloy, of 8×10^{19}/cm^3, in agreement with the results of Eq. (11).

TABLE VI. Electron hole contributions to calculated coefficients for undoped antimony.

Phen. coef.[a]	Solution 318 Hole	Solution 318 Electron	Solution 430 Hole	Solution 430 Electron
σ_{11}	15.4	5.8	14.7	7.9
σ_{33}	13.0	17.7	14.2	12.7
$-P_{123}$	1.23	−0.25	1.23	−0.25
$-P_{231}$	2.79	−1.45	2.82	−1.47
$2B_{13}$	5.53	0.42	5.27	0.57
$2B_{31}$	10.6	7.5	11.09	5.45
$-2B_{44}$	2.3	0.6	2.56	0.46
B_4	25.2	4.0	24.04	6.75
B_{33}	1.16	0.17	1.73	0.02
$-4B_{24}$	6.5	0.5	6.94	−0.08
$-4B_{42}$	3.2	0.9	4.24	−0.95

[a] Units: σ, 10^3/Ω-cm; P, 10^{-1}/Ω-cm-G; B, 10^{-8}/Ω-cm-G^2.

Because of the uncertainity in and the relative smallness of the electron contributions, we have also tried to scale the alloy solutions entirely to the hole part of the pure antimony solutions. For the 0.2% alloy, the fit is definitely poor; and for the 0.8% alloy, pure antimony solution No. 430 allows such a solution, though still of lower quality than the solutions of the two-carrier scaling model.

The analysis of the experimental data in terms of the model leads to the following conclusions:

(1) Two alternative well-defined sets of mobility ellipsoids explain the pure antimony data; they have a common structure for the holes, while the electron ellipsoids differ appreciably.

(2) The alloy data can be explained by carrier densities and mobilities which scale isotropically from either undoped antimony solution, with scale factors of similar magnitude.

(3) In all cases, the hole density more than doubles, the electron density decreases to about half its original value, but both carriers still exist in the 0.8% alloy.

(4) The hole mobilities decrease with increasing tin content, whereas the electron mobilities are practically unchanged.

TABLE VII. Scaled alloy solutions and experimental alloy values.

Inverse GM coeffs.[a]	0.2% tin Exp. value	0.2% tin Scaled values Solu. 318	0.2% tin Scaled values Solu. 430	0.8% tin Exp. values	0.8% tin Scaled values Solu. 318	0.8% tin Scaled values Solu. 430
σ_{11}	23.9	20.7	22.8	25.9	22.5	22.4
σ_{33}	26.1	29.0	25.8	22.5	24.8	24.0
$-P_{123}$	1.20	0.90	0.91	0.90	0.60	0.71
$-P_{231}$	1.25	1.28	1.39	1.01	1.16	1.26
$2B_{13}$	5.2	4.82	4.15	3.0	2.02	2.10
$2B_{31}$	14.0	14.5	12.6	6.0	6.89	6.13
$-2B_{44}$	2.02	2.4	2.2	0.86	1.03	1.08
B_4	21.0	24.3	22.2	9.8	10.51	13.0
B_{33}	1.2	1.08	1.23	0.54	0.46	0.62
$-4B_{24}$	4.8	5.68	4.80	2.64	2.34	2.48
$-4B_{42}$	4.24	3.36	2.21	2.00	1.47	1.20

[a] Units: σ, 10^3/Ω-cm; P, 10^{-1}/Ω-cm-G; B, 10^{-8}/Ω-cm-G^2.

VI. DISCUSSION

In this section we review various properties of the pure antimony solutions in order to estimate their reliability, and extend a similar estimate to the alloy solutions. We propose locations of the bands and compare our models with those proposed by others. The new information gained from the alloy data on the electronic properties of antimony is then summarized.

Our pure antimony solution 430, Table IV, agrees with F-J's solution within small differences in the values of the parameters. All major features, such as the relative sizes and magnitudes of the mobilities and the tilt angles, are recognizable, if, as we have already done in Table IV, their "2" and "3" mobilities are interchanged and the complementary tilt angles specified. [Such a transformation only changes the signs of B_{24} and B_{42} which is to be expected when the reference system is changed. See Eqs. (7).]

This good agreement is somewhat surprising in view of the differences in experimental values for the input σ's and P's. However, it is not accidental, for these solutions are characteristic of the whole neighborhood, and vary relatively smoothly with the input data. One

TABLE VIII. Alloy representative scaling factors and carrier contribution.[a]

% Sn	Holes $r_h\equiv P/N_0$	Holes $w_h\equiv \nu_i/\nu_i(0\%)$	Electrons $r_e\equiv N/N_0$	Electrons $w_e\equiv \mu_i/\mu_i(0\%)$	Carrier contribution per tin atom
0	1.0	1.0	1.0	1.0	···
0.2	1.3	0.84	0.8	0.98	0.27
0.8	2.5	0.52	0.5	0.92	0.33

[a] Units: $N_0=4.3\times10^{19}$/cm^3; ν_i, $\mu_i=(0.1$ to $4)\times10^3$ cm^2/V-sec.

may conclude that within rather wide variations of the input data a basic pattern of the parameters satisfies all the requirements imposed by the model. Similarly, this relationship also establishes the adequacy of the machine search procedure. Furthermore, the fact that the hole structure is common not only to our two solutions, but also to F-J's, is good evidence about its reality, and we conclude that these experiments define the major features of the hole ellipsoids with some certainty. However, the exact values for the mobilities and, in many cases, for the tilt angle are sensitive to the computer search parameters.

Although solution-430 electron bands are also in agreement with F-J's solution, their reality is much less certain than that of the holes. Solution 318 gives a very different answer for the electrons, and other good solutions usually show a larger variation in the ellipsoid parameter values for electrons than for holes. Furthermore, many electron solutions are near one or another of the existence limits of their parameters where the machine computation accuracy is very low. Because of this, structures whose the electron tilt angles are at either 0° or 90° may be automatically rejected by the machine and solutions having values close to either limit are an indication that such extremal solutions may exist. Moreover, a family of electron structures has not been explored in which the "2" and "3" mobilities of the electrons are interchanged, the complementary tilt angle designated, while the respective hole parameters remain fixed. This transformation is not equivalent to a reference frame change and leads to changes in the sign of the electron contributions to B_{24} and B_{42}. An examination of the contributions to B_{24} and B_{42}, Table VI, shows that the electron parts are not more than roughly 25% of the hole contributions. Adding or subtracting such small quantities neither materially improves nor worsens the general fit. The possibility of such additional solutions together with the ones already found leaves considerable uncertainty in the specification of the electrons.

The placement of the ellipsoids in the Jones zone by matching the tilt angle to the normal direction of a zone face allows various possibilities. Our hole structures, as well as F-J's, may be placed at the center of the (221) faces. The electron structure of solution 430 can also be located at this point, using the complementary tilt angle, so that overlapping bands obtain at the same point in reciprocal space. Such overlapping, predicted for reflection symmetry points of sixfold multiplicity,[13] would require doubling the number of ellipsoids, with each pair symmetrically displaced about or along the reflection plane trace. Our data allow equally well either set of ellipsoids at the centers of the (110) faces. These centers are also suitable locations for the electron part of solution 318, of tilt angle 10°. If this angle should really be 0°, the structure would have rotational symmetry and could be either along the zone axis, as suggested independently by Mase and Harrison,[14] at points of single or double multiplicity, or both, and/or at the intersections of adjacent (110) faces, with their "3" axes parallel to the trigonal direction.

Our interpretation of the alloy data is subject to all the uncertainties of the pure antimony solutions from which it is derived and, in addition, must be judged in light of the rather arbitrary assumptions inherent in our procedure of scaling the solutions. As shown in Sec. V, the pure antimony solutions can be scaled by changes in carrier density and by proportional changes of each carrier's mobilities to give a fit to the experimental alloy data. The fit is not intrinsically poorer than the unscaled fit to the pure antimony data, so that the alloy solutions obtained in this fashion have the same quality as that found by the computer for pure material. Better fitting nonscaling solutions which may be related to the pure antimony solutions found perhaps also exist. However, in terms of the model, it would be surprising if the alloy data are, indeed, more exactly interpretable than those of the pure material, for the model takes no explicit account of, for instance, impurity scattering or fluctuations about homogeneity[15] which may have an effect on the observed coefficients. Nonscaling solutions of the same quality also cannot be ruled out. (Although a formalism for searching for such solutions was set up, and trial hand calculations were carried out, we have no information on nonscaling good solutions. A search for such solutions is continuing.)

The new information obtained from the alloy measurements concerns the changes in carrier concentration with doping. From these it is possible to draw some additional conclusions about the band structure of antimony. As tin is added, the density of holes increases, while that of electrons decreases, Table VIII. The difference between the carrier densities is much smaller than the density of tin added. Thus for the 0.8% alloy, adding 26×10^{19} tin atoms/cm^3 produces a carrier unbalance of only 8×10^{19}/cm^3. A discrepancy between these numbers is not surprising, in view of the similar differences in the effect of doping on other properties of antimony and bismuth already mentioned in Sec. I. Within the uncertainties of our results, we may conclude that tin contributes about 0.3 hole per atom when added dilutely to antimony.

The fact that the hole population increases much faster than the electron population decreases implies that the density of states in the two bands differs. Employing degenerate statistics and overlapping ellipsoidal bands of standard and inverted form, and assuming that on dilute alloying (1) no relative shift of the band edges occurs, (2) the effective masses are essentially unchanged, and (3) for the 0.8% alloy, the number of holes about doubles while the number of

[13] M. H. Cohen, Phys. Rev. **121**, 387 (1961).

[14] S. Mase, J. Phys. Soc. Japan **13**, 434 (1957); **14**, 584 (1959); W. A. Harrison, J. Phys. Chem. Solids **17**, 171 (1960).

[15] C. Herring, J. Appl. Phys. **31**, 1939 (1960).

electrons is halved, we obtain for the ratio of the Fermi energy (measured with respect to the band edge) in pure antimony

$$\epsilon_e/\epsilon_h = m_h/m_e \sim 2,$$

and a hole density of states about 2.2 times that of the electrons at the Fermi level of pure antimony. Our estimates for the separate overlap and carrier Fermi energies are based on the low-temperature effective mass values available.[2] With Shoenberg's values $(m_1m_2m_3)^{1/3} = 0.17m_0$. If assigned to electrons, as cyclotron resonance experiments suggest,[16] the overlap energy for three ellipsoids is 0.19 eV, and the hole and electron Fermi energies are, respectively, 0.06 and 0.13 eV for pure antimony and 0.10 and 0.08 eV for the 0.8% alloy. The principal scattering times at room temperature are of order of magnitude 10^{-13} sec. F-J obtained an isotropic relaxation time by attributing the masses to the holes. For such an assignment we find for the overlap energy 0.42 eV, and the hole and electron Fermi energies are, respectively, 0.13 and 0.29 eV for pure antimony. These energies may be judged to be not in line with Jain's[17] gap and overlap energy variation for the Bi-Sb alloys, provided an extrapolation of his limited data to pure antimony is meaningful. Additional evidence for an electron assignment is the hole band mass of $\sim 0.34m_0$ that our model yields. This value, while it cannot be resolved into principal mass components, is approximately the cyclotron resonance mass Datars[18] tentatively ascribes to heavy holes.

Irrespective of assignment, our assumptions about the form of the bands and their relative positions, together with our result that 0.3 carrier are removed for each tin atom added, predict that about 2% tin in antimony is required to establish conduction by holes only. Some support for this figure may be found in the change of resistivity with added tin by Lane and Dodd,[10] where at about 1.2% ρ_{11} at room temperature begins to increase after passing through a minimum, indicating the turning point of two competing mechanisms.

By their nature the alloy solutions considered do not add information about the topology of the band structure, though the existence of a common mobility scaling factor for each carrier type corroborates that it remains unchanged. Based on the mobilities, τ for holes decreases rapidly with hole density whereas that for electrons remains essentially constant, in agreement with the behavior expected from degenerate carriers of low density.

The over-all agreement between the experimental data and reasonable values for the parameters of our model, including their changes with alloying, indicates that galvanomagnetic measurements on antimony can be successfully interpreted in terms of a multiple ellipsoid two-band model. A more detailed interpretation, while possible in principle, is not justified by the data and their margins of error, unless it leans also on independent information about features of the band structure, especially the effective masses of the carriers.

ACKNOWLEDGMENTS

We wish to thank Dr. S. J. Freedman of the Polytechnic Institute of Brooklyn for making his computer program available, J. W. Mellichamp of USAELRDL for the spectroscopic analyses, John Spellman, formerly Lieutenant in charge of the Automatic Data Processing Systems Computer Laboratory, U. S. Army Signal School, Ft. Monmouth, for modifying and running it, and the Signal School for the use of their IBM 650 computer. We would like to express our appreciation to both Dr. H. Jacobs, Deputy Director of the Solid State and Frequency Control Division of USAELRDL, and F. A. Brand, Chief of the Division's Microwave and Quantum Electronics Branch, for their continued encouragement and support.

[16] W. R. Datars, Phys. Rev. **124**, 75 (1961).
[17] A. L. Jain, Phys. Rev. **114**, 1518 (1959).
[18] W. R. Datars, Can. J. Phys. **39**, 1922 (1961).